

G2C: A Generator-to-Classifier Framework Integrating Multi-Stained Visual Cues for Pathological Glomerulus Classification

Bingzhe Wu*¹
wubingzhe@pku.edu.cn

Xiaolu Zhang²
yueyin.zxl@antfin.com

Shiwan Zhao³
zhaosw@cn.ibm.com

Lingxi Xie⁴
198808xc@gmail.com

Caihong Zeng⁵
zengch_nj@hotmail.com

Zhihong Liu⁵
liuzhihong@nju.edu.cn

Guangyu Sun¹
gsun@pku.edu.cn

¹ Peking University
Beijing, China

² Ant Financial
Hangzhou, China

³ IBM Research
Beijing, China

⁴ The Johns Hopkins University
Baltimore, USA

⁵ Nanjing University
Nanjing, China

* This work was done when Bingzhe Wu was a research intern at IBM Research - China.

Abstract

Pathological glomerulus classification plays a key role in the diagnosis of nephropathy. As the difference between different subcategories is subtle, doctors often refer to slides from different staining methods to make decisions. However, creating correspondence across various stains is labor-intensive, bringing major difficulties in collecting data and training a vision-based algorithm to assist nephropathy diagnosis.

This paper provides an alternative solution for integrating multi-stained visual cues for glomerulus classification. Our approach, named **generator-to-classifier** (G2C), is a two-stage framework. Given an input image from a specified stain, several *generators* are first applied to estimate its appearances in other staining methods, and a *classifier* follows to combine these visual cues for decision making. These two stages are optimized in a joint manner. To provide a reasonable initialization for the generators, we train an unpaired image-to-image translation network for each stain, and fine-tune them with the classifier. Since there are no publicly available datasets for glomerulus classification, we collect one by ourselves. Experiments reveal the effectiveness of our approach, including the authenticity of the generated patches so that doctors can hardly distinguish them from the real ones. We also transfer our model to a public dataset for breast cancer classification, and outperform the state-of-the-arts significantly.

1 Introduction

More than 10% people all over the world suffer nephropathy [1]. An important way of diagnosis lies in a quantitative analysis of glomeruli, *e.g.*, discriminating between normal and abnormal samples, and further diagnosing the abnormality if necessary. In clinics, pathologists generally refer to multiple slides of the same glomerulus, generated by different staining methods, in order to collect cues from particular glomerular structures, elements, or even microorganisms to detect subtle differences among these subcategories. In this work, we consider four staining methods, namely PAS, H&E, MASSON and PASM. As shown in Figure 1, these staining methods produce quite *different* appearances even for the *same* glomerulus.

This paper aims at designing an algorithm to integrate multi-stained visual cues. The main difficulty lies in the lack of annotation, *i.e.*, in both training and testing, labeling every glomerulus across different stains is both labor-intensive and error-prone. In our case, we are provided a partially labeled dataset on one stain (PAS), and unlabeled data on other three stains. For most glomeruli, it is difficult to find perfect snapshots in all four stains, thus we cannot expect a simple algorithm to create correspondence across different stains. This partly limits previous work [2][3] from training classification models on multiple stains.

To this end, we propose an approach named **generator-to-classifier** (G2C). The core idea is to generate fake images in other stains to assist classification. G2C has two stages. The first stage contains a few *generators*, each of which takes an input patch from the source (PAS) stain and estimates its appearance in another (*e.g.*, H&E, MASSON or PASM) stain. The second stage builds a *classifier* upon all stains, one real and a few generated, and outputs prediction. Compared to the recent work [24] which generated images of higher quality to train more powerful models, our work provides an alternative way to assist deep network optimization with generated image data.

We suggest to optimize G2C in a joint manner so as to facilitate the collaboration between these two stages. To provide a reasonable initialization for the generators, we make use of CycleGAN [25] to perform unpaired image-to-image translation given weakly labeled training data. Experiments reveal significant improvement brought by our approach on glomerulus classification. In addition, we directly apply our approach to breast cancer images, showing its satisfying transferability across different diseases.

We diagnose the effectiveness of G2C with a few comparative studies. **First**, we find it difficult even for the doctors to discriminate the generated glomerulus patches from the real ones, suggesting that the generators are producing reasonable multi-stained information. **Second**, joint optimization over the generators and the classifier brings a consistent accuracy gain, verifying the value of coupling information. **Third**, the generation stage can be explained as an advanced way of data augmentation, which provides more training data to alleviate over-fitting in the classification stage.

The remainder of this paper is organized as follows. We first briefly review related work

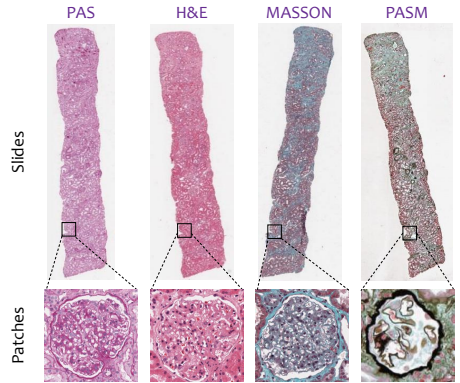


Figure 1: Top: slides from four different staining methods (PAS, H&E, MASSON and PASM). Bottom: four real patches, containing the *same* glomerulus, sampled from the *same* position of these slides.

in Section 2, and then illustrate the generator-to-classifier (G2C) framework in Section 3. After experimental results are shown in Section 4, we conclude this work in Section 5.

2 Related Work

Computer-aided diagnosis (CAD) plays a central role in assisting human doctors for clinical purposes. One of the most important prerequisites of CAD is medical imaging analysis, which is aimed at processing and understanding CT, MRI and ultrasound images in order to diagnose human pathology. In comparison, the digital pathology (DP) provides more accurate imaging in a small region of body tissues. Recent years have witnessed an explosion in this field, which is widely considered as one of the most promising techniques in the diagnosis, prognosis and prediction of cancer and other important diseases. This paper studies glomerulus classification from DP images. This is a key technique in diagnosing nephropathy, one of the most common types of diseases in the world.

In the conventional literatures, people made use of handcrafted features to capture discriminative patterns in digital pathology images. For example, [14] applied an SVM on top of the Rectangular Histogram-of-Gradients (R-HOG) features for glomerulus detection, and [9] designed Fuzzy Color Histogram (FCH) features [10] to identify subcategories of breast cancer. Recently, the rapid development of deep learning brought more powerful and efficient solutions. Especially, as one of the most important models in deep learning, the convolutional neural networks [16][25][26] have been applied to a wide range of tasks in medical imaging analysis, including classification [9] [6] [7], detection [8], segmentation [22], *etc.* In the field of DP image processing, [20] designed an automatic method to detect cancer metastases, which outperformed human doctors. [2] proposed a coarse-to-fine approach for mitosis detection. In [13], a unified framework was presented for a series of tasks, including nuclei segmentation and mitosis detection. Our work is closely related to [20], which trained deep networks to outperform handcrafted features in glomerulus classification.

The importance of using multiple stains for digital pathology diagnosis is emphasized by the doctors in our team. However, annotating data correspondence is difficult and time-consuming, so we turn to the family of Generative Adversarial Networks (GANs) [8] to perform image-to-image translation. There are generally two types of translation algorithms, paired [12] and unpaired [15][19][27][28], which differ from each other in the organization of input data. The former type is often more accurate, while the latter type can be used in the scenario of missing data correspondence, which fits the requirement of this work.

3 Approach

3.1 Backgrounds

Staining is used to highlight important features of a soft tissue. Each staining method has both advantages and disadvantages [8]. For example, the PAS stains glomerular basement membranes, mesangial matrix and tubular basement membranes red (positive), while the PASM colors the same component black, providing a clear contrast between positively and negatively staining structures. Integrating multi-stained information is very important for pathology image analysis, *e.g.*, for clinical purposes.

However, in collecting a large dataset for glomerulus classification, it is difficult to label each glomerulus under all staining methods, because (i) finding correspondence between

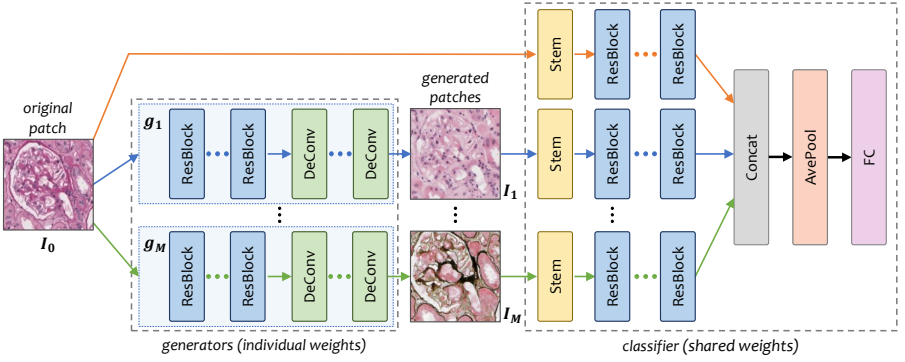


Figure 2: The overall **generator-to-classifier** (G2C) framework. The left part illustrates the M *generators*, and the right part the *classifier*, in which all $M + 1$ branches share the same weights. When an input patch comes, m other stains are generated, and then combined with the original one for classification. The entire framework is end-to-end, and all the modules can be optimized in a joint manner.

stains is labor-intensive, and (ii) only a small portion of glomeruli can be clearly seen in multiple stains¹. Therefore, we set our goal to be *glomerulus classification from single-stained inputs*. To be specific, each input patch contains a glomerulus from the PAS stain. Meanwhile, a small corpus of 100 unlabeled patches from each of the other three stains is also provided as the reference set (used for initializing generators).

3.2 Formulation

We formulate single-stained glomerulus classification into a joint optimization task, in which a few *generators* are first used to generate other stains (H&E, MASSON and PASM) from the input PAS stain, and a *classifier* follows to extract features from all these images and outputs the final prediction.

Let an input image be \mathbf{I} , which is a patch sampled from a slide with PAS staining. The goal is to design a model $\mathbb{M} : t = \mathbf{f}(\mathbf{I}; \theta)$, where t is a class label, and θ are the model parameters, *e.g.*, the learnable weights in the convolutional neural networks. Following the above idea, we decompose the model into two modules, generation and classification. The overall flowchart is illustrated in Figure 2.

• The Generation Network

The first module, one or few *generators*, play the role of generating images of different staining methods from the input image \mathbf{I} . We denote the generated set by $\mathcal{I} = \{\mathbf{I}_0, \mathbf{I}_1, \dots, \mathbf{I}_M\}$, in which $\mathbf{I}_0 \doteq \mathbf{I}$ is the source image, and all other M ones are generated using a parameterized model $\mathbf{I}_m = \mathbf{g}_m(\mathbf{I}_0; \theta_m^G)$, $m = 1, 2, \dots, M$.

Each generator consists of several down-sampling units (residual [10] and pooling layers) and several up-sampling layers (de-convolutional layers). In experiments, we observe that classification accuracy goes up with the number of residual blocks and gradually saturates. In practice, we use 9 residual blocks in all our experiments. In addition, we insert an instance normalization layer after each convolutional layer, following [28].

¹ Each slide in digital pathology can be stained only once. Even if a set of neighboring slides containing the same glomerulus are used in various stains, its appearance may not be identical due to the difference in slicing positions.

• The Classification Network

The second module, a *classifier*, extracts features from the source image and the generated ones for classification. Mathematically, it can be formulated as $t = \mathbf{c}(\mathbf{I}_0, \mathbf{I}_1, \dots, \mathbf{I}_M; \theta^C)$. As illustrated in the next subsection, this is a multi-path model consisting of $M + 1$ sub-networks, which share the same set of parameters (θ^C) to extract features from different staining images.

More specifically, the classification network C can be divided into two parts: $M + 1$ weight-sharing back-end networks for extracting image features, and a front-end network for concatenating extracted feature vectors and making the final prediction. Each back-end network is a variant of the deep residual network [14], in which the first convolutional layer with a window size of 7×7 is replaced by a stem block [26], which consists of three convolution blocks followed by a 2×2 max-pooling layer. Experiments show that using the stem block consistently improves classification accuracy by more than 1%.

In overall, the overall framework is a composed function of the generator and the classifier, *i.e.*, $t = \mathbf{f}(\mathbf{I}; \theta) \doteq \mathbf{c} \circ \mathbf{g}(\mathbf{I}; \{\theta_m^G\}_{m=1}^M, \theta^C)$. Note that when $M = 0$, our model degenerates to that using one single stain for classification. Sharing parameters over $M + 1$ branches enables us to fairly compare our model and the baseline *at the classification stage*. This idea also originates from the doctors in our team, who suggests that different staining images provide complementary information in diagnosis, but the basic principles to recognize them should remain unchanged.

3.3 Optimization

The benefit of jointly optimizing $t = \mathbf{c} \circ \mathbf{g}(\mathbf{I}; \{\theta_m^G\}_{m=1}^M, \theta^C)$ is to enable the parameters of the generators and the classifier to collaborate with each other. But, according to our motivation, the generator should be able to produce some reasonable images corresponding to other staining methods. Therefore, we suggest a two-stage training process, in which we first train the generative networks using some unlabeled data covering different stains, and then fine-tune the generator together with the classifier towards higher recognition accuracy.

• Initializing the Generators

Due to the lack of data correspondence, the generators are initialized by a task known as unpaired image-to-image translation. 100 patches from the source stain and another 100 from the target stain are provided. Note that all these patches are unlabeled, and may even not contain glomeruli. We use a recent approach named CycleGAN [28], which trains a reverse generator, denoted by $\hat{\mathbf{g}}_m$, to translate the patches generated by \mathbf{g}_m back to the source stain. $\hat{\mathbf{g}}_m$ shares the same structure with \mathbf{g}_m . We follow the original implementation.

Note that, if additional annotations on the target domains are available, we can use more accurate image-to-image translation algorithms such as [12] to initialize our model.

• Fine-tuning Generators with the Classifier

In this stage, we train the classifier together with the generators in a fully-supervised manner (each glomerulus is assigned a class label). **In this stage, our goal is no longer high-quality generation, but accurate classification.** Therefore, the unlabeled data from other stains are not used, and all the generators $\hat{\mathbf{g}}_m$, $m = 1, \dots, M$, are simply discarded.

In network training, we use Stochastic Gradient Descent with a momentum of 0.5. We perform a total of 30 epochs. The learning rate is set to be 0.01 at the beginning, and divided by 10 after every 5 epochs. In the first 5 epochs, we freeze all parameters in the generators

in order to initialize the classifier with fixed generated samples, so as to improve the stability in training. Note that freezing the generators in all 30 epochs leads to training the generators and the classifier individually. We shall show in Section 4.3 that joint optimization leads to significant accuracy gain over all our generator-to-classifier models.

As we shall see in Section 4.1, data distribution is imbalanced in our dataset. To prevent a category with fewer training samples from being swallowed by another category, we introduce the focal loss function [18] which brings slight but consistent accuracy gain in each individual classification task.

3.4 Why Our Approach Works?

It remains to discuss why our algorithm works well (see Section 4 for quantitative results). The key contribution naturally comes from the ability of simulating different staining methods, and enabling jointly optimization so that the classifier takes advantage of complementary information. To confirm that these information comes from the *authenticity* of the generators, we perform a user study (see Section 4.3), revealing the difficulty, even for the professional doctors in our team, to discriminate the generated and real patches.

Moreover, we make some comments on another question: as all the information comes from the input image (*i.e.*, either in the baseline or our algorithm, the classifier sees the same amount of information), what is brought into the system that leads to the accuracy gain? We explain this to be a guided way of extracting high-quality features. Note that in training a glomerulus classifier, the amount of data is most often very limited. Our dataset merely contains 2,650 cases for *ss-vs-gs* classification, with less than 1,000 training images in the *ss* subtype. When a powerful classifier, say a very deep neural network, is used, the training data can be explained in a lot of different ways, but most of them do not learn from human knowledge, and thus do not fit the testing data very well. Our algorithm, by introducing the knowledge from human doctors that other staining methods are helpful to classification, forces the model to rely a great deal on multi-stained data. We believe this algorithm to endure fewer risks especially in the scenario of limited data. This is verified by investigating the over-fitting issue, shown in Section 4.3, and transferring our models to another dataset for breast cancer classification, shown in Section 4.4.

4 Experiments

4.1 Dataset and Settings

We collect a dataset for glomerulus classification. As far as we know, there is no public dataset for this purpose (existing ones [21] worked on glomerulus-vs-non-glomerulus classification). Our dataset is collected from 209 patients, each of which has several slides from four staining methods, namely PAS, H&E, MASSON and PASM. In all PAS slides, we ask the doctors to manually label a bounding box for each glomerulus, and annotate its subcategory. The doctors annotate with confidence, *i.e.*, only those PAS patches containing enough information to make decisions are preserved. The subcategories include *global sclerosis (gs)*, *segmental sclerosis (ss)*, and being normal (*none of the above* or *noa*).

	<i>ss</i>	<i>gs</i>	<i>noa</i>	Total
Training	648	2,002	7,000	9,650
Testing	237	618	2,828	3,683
Total	885	2,620	9,828	13,333

Table 1: Number of annotated glomeruli of each subcategory in the PAS stain. The *ss* and *gs* categories compose the high-level abnormal category, denoted by *s*.

	<i>s</i>	<i>noa</i>	Avg
PAS_ONLY	90.76	90.73	90.74
PAS_H&E	92.74	92.36	92.55
PAS_MASSON	92.39	91.72	92.06
PAS_PASM	93.09	91.83	92.46
PAS_ALL	93.68	92.99	93.34

Table 2: Category-wise and averaged classification accuracies (%) in the *s*-vs-*noa* task.

	<i>ss</i>	<i>gs</i>	Avg
PAS_ONLY	78.05	96.76	87.41
PAS_H&E	79.23	96.87	88.05
PAS_MASSON	78.31	96.79	87.55
PAS_PASM	81.43	97.57	89.50
PAS_ALL	81.59	98.20	89.90

Table 3: Category-wise and averaged classification accuracies (%) in the *ss*-vs-*gs* task.

Global sclerosis and segmental sclerosis are two levels of *glomerulosclerosis* (denoted by *s*). Advised by the doctors, we consider two classification tasks, dealing with *s*-vs-*noa* and *gs*-vs-*ss*, respectively. The first task is aimed at discriminating abnormal glomeruli from normal ones, and the second task goes one step further to determine abnormality of the abnormal glomeruli. To deal with imbalanced label distribution (see Table 1), we report category-averaged accuracies [10] in the following experiments. All 209 patients in the dataset are split into a training set (149 patients) and a testing set (60 patients). There are in total 9,650 annotated patches (each contains one glomerulus) in the training set and 3,683 in the testing set. The statistics of all subcategories are provided in Table 1. As described in Section 3.3, an additional set of 100 patches for *each* stain is used for initializing the generators.

In $t = \mathbf{c} \circ \mathbf{g}(\mathbf{I}; \{\theta_m^G\}_{m=1}^M, \theta^C)$, setting $M = 0$ leads to our baseline model in which only the PAS stain is used for classification. We denote it by PAS_ONLY. We also provide several competitors, which differ from each other in the type(s) of stains generated to assist classification. These variants are denoted by PAS_H&E, PAS_MASSON, PAS_PASM and PAS_ALL, respectively. Among which, PAS_ALL integrates information from all the other three stains, *i.e.*, setting $M = 3$.

In our dataset, there are much fewer abnormal glomerulus patches than normal ones. To prevent over-fitting, we perform data augmentation by (i) randomly flipping input patches vertically and/or horizontally, and (ii) performing random color jittering, including changing the brightness and saturation of input patches. We also make use of focal loss [18] which brings consistent accuracy gain. During training, all input patches are rescaled into 224×224 , and pixel intensity values are normalized into $[0, 1]$.

4.2 Quantitative Results

• Level-1 Classification: *s*-vs-*noa*

We first evaluate classification accuracy in discriminating abnormal glomeruli (denoted by *s*) from normal ones (denoted by *noa*). Results are summarized in Table 2. One can observe that introducing additional stain(s) consistently improves classification accuracy. An interesting but expected phenomenon emerges by looking into category-wise accuracies. For example, based on the PAS stain, adding H&E produces a higher classification rate in the normal (*noa*) category, while MASSON works better in finding abnormal (*s*) glomeruli. This suggests that different stains provide complementary information to assist diagnosis, and verifies the motivation of this work. Therefore, it is not surprising that combining all other stains obtains consistent accuracy gain over other competitors. In particular, the PAS_ALL model outperforms the PAS_ONLY model by 2.60% in the averaged accuracy, or a 28.08%

	Training	Testing	Gap
PAS_ONLY	96.48	87.41	9.07
PAS_H&E	94.90	88.05	6.85
PAS_MASSON	93.23	87.55	5.68
PAS_PASM	95.03	89.50	5.53
PAS_ALL	94.87	89.90	4.97

Table 4: The results show the effectiveness of our method to prevent overfitting. The train-test represent the gap between training and testing accuracy of used models.







	F1	Acc (%)
	0.666	77.24
	0.675	78.74
	0.718	84.23
 (PAS_ONLY)	0.765	84.68
Ours (PAS_ALL)	0.842	87.54

Table 5: Comparison of F1-scores and balanced accuracies on the breast cancer classification task. We follow the baseline  to use AlexNet  for classification.

relative drop in classification error. To demonstrate the statistical significance of the achieved improvement, we collect the classification accuracy on all the 60 patients in the testing set and compute and perform the student's t -test, which reports a p -value of 0.011 ($93.31 \pm 8.14\%$ by PAS_ALL vs. $90.74\% \pm 7.25\%$ by PAS_ONLY).

• Level-2 Classification: *ss-vs-gs*

Next, we further categorize the abnormal (*s*) glomeruli into two subtypes, namely, investigating the *ss-vs-gs* classification task. Advised by the doctors in our team, we only consider those correctly categorized abnormal patches in Level-1. Results are summarized in Table 3. Qualitative analysis gives similar conclusions, *i.e.*, different stains provide complementary information, therefore it is instructive to combine all stains for accurate classification. It is worth noting that in these two abnormal subcategories, segmental sclerosis (*ss*) suffers lower accuracy compared to global sclerosis (*gs*), which is partly caused by the limited amount and imbalance of training data. This is alleviated by incorporating generated patches from other stains as augmented data. Compared to PAS_ONLY, the PAS_ALL model significantly improves the *ss* classification accuracy by 3.54%, and the overall accuracy by 2.49% (a 19.78% relative drop in classification error).

4.3 Discussions

• Visualization

To confirm the authenticity of the generated patches, we perform a study by asking the doctors in our team to discriminate the generated patches from the real ones. We sample 50 patches from all the generated ones, combine them with 50 real patches, show them one-by-one to the pathologists and record their judgments. The average accuracy over three pathologists is around 70% (random guess reports 50%), suggesting a reasonably high quality in image generation.

We visualize several examples in Figure 3. These glomeruli are misclassified

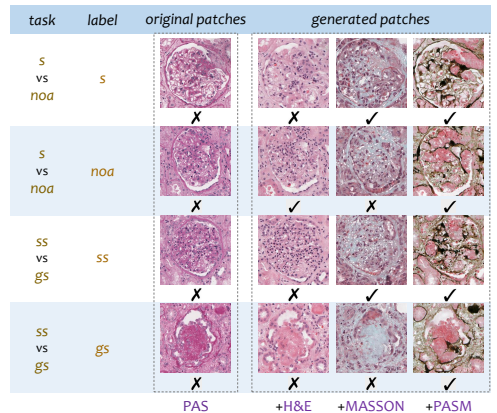


Figure 3: Different stains provide complementary information to assist glomerulus classification. In each row, the original patch is mis-classified using the PAS stain alone (marked by a \times), but turned into correctness after integrating some of other generated patches (marked by a \checkmark). All the generated

using the PAS stain alone, but rescued by the generated stains. We note that each failure case in PAS can be helped by one or a few other stains. In clinics, these generated patches may also assist doctors in case that a PAS patch does not contain sufficient information.

• Joint Optimization

In addition, joint optimization brings significant gain in classification accuracy. In comparison to the model in which the generators and the classifier are optimized individually (*i.e.*, the weights of the generators are frozen throughout the fine-tuning stage, see Section 3.3), the jointly optimized models (PAS_ALL) achieve 1.10% and 1.54% boosts on *s-vs-noa* and *ss-vs-gs* classification, respectively. In particular, the error of the most challenging *ss* class is reduced from 20.68% to 18.41% (2.27% absolute or 10.98% relative improvement).

• The Over-fitting Issue

In the area of medical imaging analysis, recognition accuracy is often limited by the insufficiency of training data. In our collected dataset, there are less than 1,000 training samples for the *ss* subcategory, raising a considerable risk of over-fitting.

Generating patches in other stains alleviates over-fitting to some extents. It provides complementary information to geometry-based data augmentation such as flip and rotation, as the generators bring in some *priors* learned from the reference sets (100×3 unlabeled patches from other stains), forcing the training data to be explained in a more reasonable manner. To verify this, we record both training and testing accuracies for each of the five models for *ss-vs-gs* classification in Table 4. Using multiple stains leads to a higher testing accuracy but a lower training accuracy, which is the consequence of a stronger constraint (multiple stains need to be explained collaboratively) in training deep neural networks.

4.4 Transferring to Breast Cancer Classification

To further demonstrate the effectiveness of our approach, we apply it to a publicly available dataset for invasive ductal carcinoma (IDC) classification², which contains 277,524 patches of 50×50 pixels (198,738 IDC-negative and 78,786 IDC-positive). To make a fair comparison, we reproduce [13] with the same network architecture (AlexNet) on the PAS stain alone. This is the baseline PAS_ONLY model. As all patches in this dataset are PAS-stained, we do not train new generators from scratch, but simply transfer the pre-trained ones from our dataset, and fine-tune them with the new classifier. This model is denoted by PAS_ALL.

Results are shown in Table 5. In terms of both F1-score and classification accuracy, our approach significantly outperforms [13], as well as two previous methods with handcrafted features [10] and relatively shallow CNNs [9]. We can of course achieve higher accuracy if more powerful neural networks are used. Hence, we conclude on the effectiveness of our training strategy. The first stage, *i.e.*, initializing the generators, can be performed in a few reference sets **only once**; when another dataset is available, we can directly move on to the second stage, *i.e.*, fine-tuning a new classifier with these generators.

²<http://www.andrewjanowczyk.com/use-case-6-invasive-ductal-carcinoma-idc-segmentation/>

5 Conclusions

In this paper, we present a novel approach for glomerulus classification in digital pathology images. Motivated by the need of generating multiple stains for accurate diagnosis, we design a **generator-to-classifier** (G2C) network, and perform an effective two-stage training strategy. **The key innovation lies in the mechanism which enables several generators and a classifier to collaborate in both training and testing.** A large dataset is collected by the doctors in our team, since there are no publicly available datasets for the same purpose. Our approach achieves considerably higher accuracies over the baseline, and transfers reasonably well to another digital pathology dataset for breast cancer classification.

This research paves a new way of data augmentation and/or enhancement in medical imaging analysis. Transferring this idea to other types of data generation, *e.g.*, integrating CT scans from the *arterial phase* and the *venous phase* for organ segmentation, is promising and implies a wide range of clinical applications.

References

- [1] K.H. Brodersen, C.S. Ong, K.E. Stephan, and J.M. Buhmann. The balanced accuracy and its posterior distribution. In *ICPR*, 2010.
- [2] H. Chen, Q. Dou, X. Wang, J. Qin, P.A. Heng, et al. Mitosis detection in breast cancer histology images via deep cascaded networks. In *AAAI*, 2016.
- [3] A. Cruz-Roa, A. Basavanthally, F. González, H. Gilmore, M. Feldman, et al. Automatic detection of invasive ductal carcinoma in whole slide images with convolutional neural networks. In *SPIE*, 2014.
- [4] Q. Dou, H. Chen, L. Yu, L. Zhao, J. Qin, et al. Automatic detection of cerebral microbleeds from mr images via 3d convolutional neural networks. *TMI*, 35(5):1182–1195, 2016.
- [5] A. Esteva, B. Kuprel, R.A. Novoa, J. Ko, S.M. Swetter, et al. Dermatologist-level classification of skin cancer with deep neural networks. *Nature*, 542(7639):115–118, feb 2017.
- [6] A.B. Fogo, A.H. Cohen, R.B. Colvin, J.C. Jennette, and C.E. Alpers. *Fundamentals of Renal Pathology*. Springer, 2014.
- [7] J. Gallego, A. Pedraza, S. Lopez, G. Steiner, L. Gonzalez, A. Laurinavicius, and G. Bueno. Glomerulus classification and detection based on convolutional neural networks. *Journal of Imaging*, 4(1), 2018.
- [8] I. Goodfellow, J. Pouget-Abadie, M. Mirza, B. Xu, D. Warde-Farley, S. Ozair, A. Courville, and Y. Bengio. Generative adversarial nets. In *NIPS*, 2014.
- [9] V. Gulshan, L. Peng, M. Coram, M.C. Stumpe, D. Wu, et al. Development and validation of a deep learning algorithm for detection of diabetic retinopathy in retinal fundus photographs. *JAMA*, 304(6):649–656, 2016.
- [10] J. Han and K.K. Ma. Fuzzy color histogram and its use in color image retrieval. *TIP*, 11(8):944–952, 2002.

- [11] K. He, X. Zhang, S. Ren, and J. Sun. Deep residual learning for image recognition. In *CVPR*, 2016.
- [12] P. Isola, J.Y. Zhu, T. Zhou, and A.A. Efros. Image-to-image translation with conditional adversarial networks. In *CVPR*, 2017.
- [13] A. Janowczyk and A. Madabhushi. Deep learning for digital pathology image analysis: A comprehensive tutorial with selected use cases. *JPI*, 7(1):29, 2016.
- [14] T. Kakimoto, K. Okada, Y. Hirohashi, R. Relator, M. Kawai, et al. Automated image analysis of a glomerular injury marker desmin in spontaneously diabetic torii rats treated with losartan. *Journal of Endocrinology*, 222(1):43–51, 2014.
- [15] T. Kim, M. Cha, H. Kim, J. Lee, and J. Kim. Learning to discover cross-domain relations with generative adversarial networks. In *ICML*, 2017.
- [16] A. Krizhevsky, I. Sutskever, and G.E. Hinton. Imagenet classification with deep convolutional neural networks. In *NIPS*, 2012.
- [17] A. Levin, M. Tonelli, J. Bonventre, J. Coresh, J.A. Donner, A.B. Fogo, et al. Global kidney health 2017 and beyond: A roadmap for closing gaps in care, research, and policy. *The Lancet*, 390(10105):1888–1917, 2017.
- [18] T.Y. Lin, P. Goyal, R. Girshick, K. He, and P. Dollár. Focal loss for dense object detection. In *ICCV*, 2017.
- [19] M.Y. Liu, T. Breuel, and J. Kautz. Unsupervised image-to-image translation networks. In *NIPS*, 2017.
- [20] Y. Liu, K. Gadepalli, M. Norouzi, G.E. Dahl, T. Kohlberger, A. Boyko, S. Venugopalan, A.N. Timofeev, P.Q. Nelson, G.S. Corrado, et al. Detecting cancer metastases on gigapixel pathology images. *arXiv preprint arXiv:1703.02442*, 2017.
- [21] A. Pedraza, J. Gallego, S. Lopez, L. Gonzalez, A. Laurinavicius, and G. Bueno. Glomerulus classification with convolutional neural networks. In *MIUA*, 2017.
- [22] O. Ronneberger, P. Fischer, and T. Brox. U-net: Convolutional networks for biomedical image segmentation. In *MICCAI*, 2015.
- [23] J. C. Rueda. A prototype system to archive and retrieve histopathology images by content. In *Master’s Thesis*, 2008.
- [24] A. Shrivastava, T. Pfister, O. Tuzel, J. Susskind, W. Wang, and R. Webb. Learning from simulated and unsupervised images through adversarial training. In *CVPR*, 2017.
- [25] K. Simonyan and A. Zisserman. Very deep convolutional networks for large-scale image recognition. In *ICLR*, 2015.
- [26] C. Szegedy, S. Ioffe, V. Vanhoucke, and A.A. Alemi. Inception-v4, inception-resnet and the impact of residual connections on learning. In *AAAI*, 2017.
- [27] Z. Yi, H. Zhang, P.T. Gong, et al. Dualgan: Unsupervised dual learning for image-to-image translation. In *ICCV*, 2017.
- [28] J.Y. Zhu, T. Park, P. Isola, and A.A. Efros. Unpaired image-to-image translation using cycle-consistent adversarial networks. In *ICCV*, 2017.